Regulation of proximal T cell receptor signaling and tolerance induction by deubiquitinase Usp9X

Edwina Naik,[1] Joshua D. Webster,[2] Jason DeVoss,[3] Jinfeng Liu,[4] Rowena Suriben,[1] and Vishva M. Dixit[1]

[1]Department of Physiological Chemistry, [2]Department of Pathology, [3] Department of Immunology, [4] Department of Bioinformatics and Computational Biology, Genentech, Inc., South San Francisco, CA 94080

The T cell hyperproliferation and autoimmune phenotypes that manifest in mice lacking E3 ubiquitin ligases such as Cbl, ITCH, or GRAIL highlight the importance of ubiquitination for the maintenance of peripheral T cell tolerance. Less is known, however, about the deubiquitinating enzymes that regulate T cell proliferation and effector function. Here, we define a cell intrinsic role for the deubiquitinase Usp9X during proximal TCR signaling. Usp9X-deficient T cells were hypoproliferative, yet mice with T cell–specific *Usp9x* deletion had elevated numbers of antigen-experienced T cells and expanded PD-1 and OX40-expressing populations consistent with immune hyperactivity. Aged *Usp9x* KO mice developed lupus-like autoimmunity and lymphoproliferative disease, indicating that ubiquitin ligases and deubiquitinases maintain the delicate balance between effective immunity and self-tolerance.

CORRESPONDENCE
Vishva M. Dixit:
dixit@gene.com

Abbreviations used: ANA, antinuclear antibodies; CBM, CARMA1–Bcl10–MALT1; DN, double-negative; DP, double-positive; dsDNA, double-stranded DNA; HSC, hematopoietic stem cell; NZB/W, New Zealand black/white; SLE, systemic lupus erythematosus; SP, single-positive; ssDNA, single-stranded DNA; Usp9X, ubiquitin-specific protease 9X.

Ignorance of self-antigens is one example of a cell intrinsic mechanism for inducing tolerance in peripheral T cell populations and results from either a failure to encounter self-antigens or more pertinently, because the avidity or amount of self-antigen is not sufficient to trigger a response. Naive $CD4^+$ T cells function at the apex of the adaptive immune response, where, during an initial encounter with antigen, their principal function is to discriminate between low and high signal strength. If a signal is high, as is typically the case for encounters with foreign antigens, then the antigen-specific T cell will undergo clonal expansion; however, if the signal strength is low, an immune response fails to occur. Insights into the regulation of the earliest signaling events downstream of TCR engagement will inform our understanding of how signal strength is modulated during this critical decision making process.

The enzymatic conjugation of the 76-aa protein ubiquitin to lysine residues, either singly or as polymeric chains, impacts cell signaling by modifying the stability, localization, or interactions of a protein (Komander and Rape, 2012). Ubiquitin is attached by the concerted actions of E1, E2, and E3 enzymes and it is removed by ubiquitin hydrolases (also called deubiquitinating enzymes). Therefore, the balance between these activities will determine the magnitude and duration of signaling. The E3 ubiquitin ligases Cbl, ITCH, and GRAIL are established regulators of peripheral T cell tolerance due to their provision of negative signals that shift the balance toward lower TCR signal strength. For example, in activated peripheral T cells, Cbl-b binds and ubiquitinates the TCR-proximal kinase ZAP70, resulting in its proteasomal-mediated degradation (Lupher et al., 1996; Rao et al., 2000). The fact that deubiquitinating enzymes counteract these ligases to shift the balance toward higher signal strength has received little attention.

Ubiquitin-specific protease 9X (Usp9X) is a mammalian orthologue of the *Drosophila* developmental gene *fat facets* (Wood et al., 1997) that exhibits specificity for diverse ubiquitin linkages, not only removing degradative K48-linked ubiquitin chains (Nagai et al., 2009; Schwickart et al., 2010) but also nondegradative monoubiquitin from SMAD4 (Dupont et al., 2009) and atypical Lys29/33 polyubiquitin chains from NUAK1 or

The Rockefeller University Press $30.00
J. Exp. Med. 2014 Vol. 211 No. 10 1947-1955
www.jem.org/cgi/doi/10.1084/jem.20140860

MARK4 (Al-Hakim et al., 2008). Here, we show that Usp9X is a positive regulator of proximal TCR signaling in peripheral T cells and also contributes to T cell tolerance established during intrathymic development.

RESULTS AND DISCUSSION

Usp9X protein is expressed in lymphocytes

Western blots of mouse tissues revealed abundant Usp9X in the brain and appreciable expression in the lung, spleen, lymph nodes, and thymus (Fig. 1 A). *Usp9x* knock-in mice expressing the fusion protein tdTomato-T2A-Usp9X allowed a more detailed analysis of *Usp9x* mRNA expression in the hematopoietic compartment (Fig. 1 B). The self-cleaving T2A peptide (Ryan et al., 1991) liberated the fluorescent tdTomato protein, which was detected by flow cytometry in hematopoietic stem cells (HSCs) and, to a lesser extent, in differentiated myeloid and lymphoid cells (Fig. 1 C). These data are reminiscent of in situ hybridization analyses where expression of *Usp9x* during embryogenesis decreased as cell-fate became restricted (Wood et al., 1997). Although tdTomato mRNA was expressed similarly in myeloid and lymphoid cells (Fig. 1 C), T and B cells contained significantly more Usp9X protein than granulocytes and monocytes (Fig. 1 D), which is consistent with posttranslational regulation of Usp9X protein abundance.

Usp9X regulates proximal TCR signaling events

Neither *Usp9x*$^{-/y}$ nor *Usp9x*$^{+/-}$ mice survived embryogenesis, so we explored Usp9X function in lymphoid cells from mice bearing *Usp9x* conditional KO alleles that were deleted in hematopoietic cells with a *vavCre* transgene or in T cells with a CD4.cre transgene (Fig. 2 A). Naive *Usp9x* KO CD4$^+$ T cells exhibited a proliferation defect when cultured with antibodies to CD3 and CD28, incorporating significantly less [^{3}H]-thymidine than their WT counterparts (Fig. 2 B). As *Usp9x* KO CD4$^+$ T cells proliferated normally in response to PMA and ionomycin (Fig. 2 C), which directly activate PKCθ and elevate intracellular calcium, it can be concluded that Usp9X regulates proximal TCR signaling events. The TCR-dependent proliferation defect was not secondary to altered development in the absence of Usp9X because wild-type CD4$^+$ T cells exhibited the same defect after siRNA knockdown of *Usp9x* in culture (Fig. 2 D). It is worth noting that the proliferation defect caused by Usp9X deficiency was observed in CD8$^+$ T cells as well as CD4$^+$ T cells (Fig. 2 E). Although *Usp9x* KO T cells expressed normal amounts of TCR/CD3 on their surface (Fig. 2 A) and phosphorylated the proximal kinase ZAP70 normally in response to TCR engagement (Fig. 2 F), phosphorylation of the ZAP70 substrates LAT, Vav, and Slp-76 was markedly reduced when compared with WT control T cells (Fig. 2 F). Therefore, Usp9X is required for transduction of the activation signal from ZAP70 to its substrates. Whether Usp9X targets ZAP70 directly or indirectly remains to be determined. Of note, PKCθ-dependent phosphorylation of CARMA1, subsequent binding of CARMA1 to Bcl10, and the nuclear translocation of the p65 NF-κB subunit occurred normally in *Usp9x* KO T cells (Fig. 2, G–I). Consequently, our genetic and biochemical data do not support the reported model wherein the role of Usp9X during T cell activation is to modulate the CARMA1–Bcl10–MALT1 (CBM) complex downstream of PKCθ (Park et al., 2013).

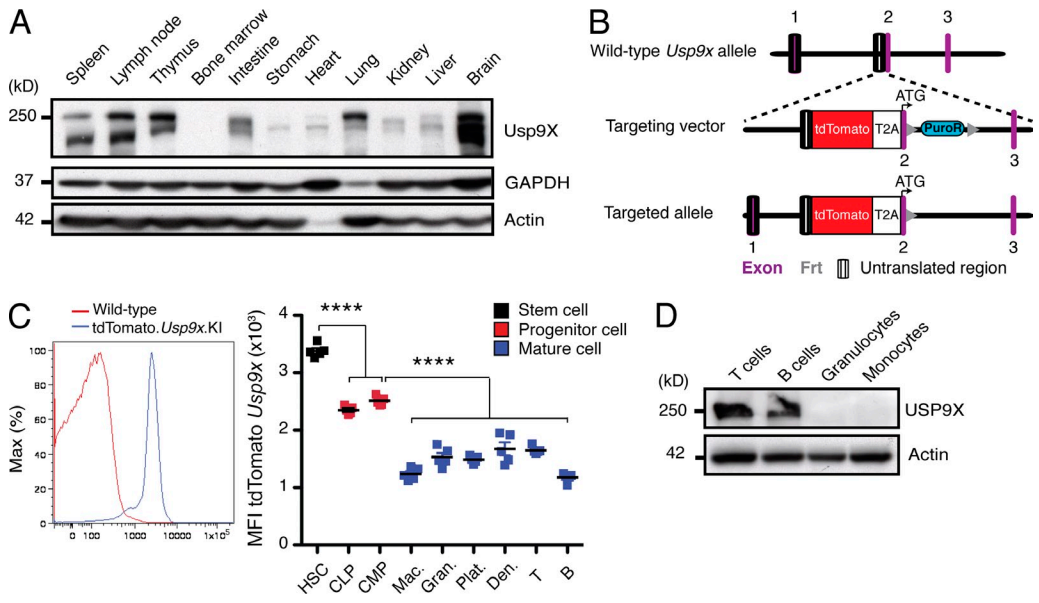

Figure 1. Usp9X protein is expressed in lymphocytes. (A) Usp9X protein expression in a panel of adult murine tissues. (B) Organization of the tdTomato.*Usp9x* knock-in allele. (C) Representative histogram and collated MFI (median fluorescence intensity) of tdTomato.*Usp9x* mRNA. CMP, common myeloid progenitor; CLP, common lymphoid progenitor; Mac, monocyte/macrophage; Gran, granulocyte; Plat, platelets; Den, dendritic cells; T and B, T and B lymphocytes. (D) Usp9X protein expression in hematopoietic cell subsets. All experiments were conducted a minimum of two independent times with littermate controls on a C57BL/6 background. Each square represents an independent mouse. ****, $P \leq 0.0001$ using a two-tailed unpaired Student's *t* test.

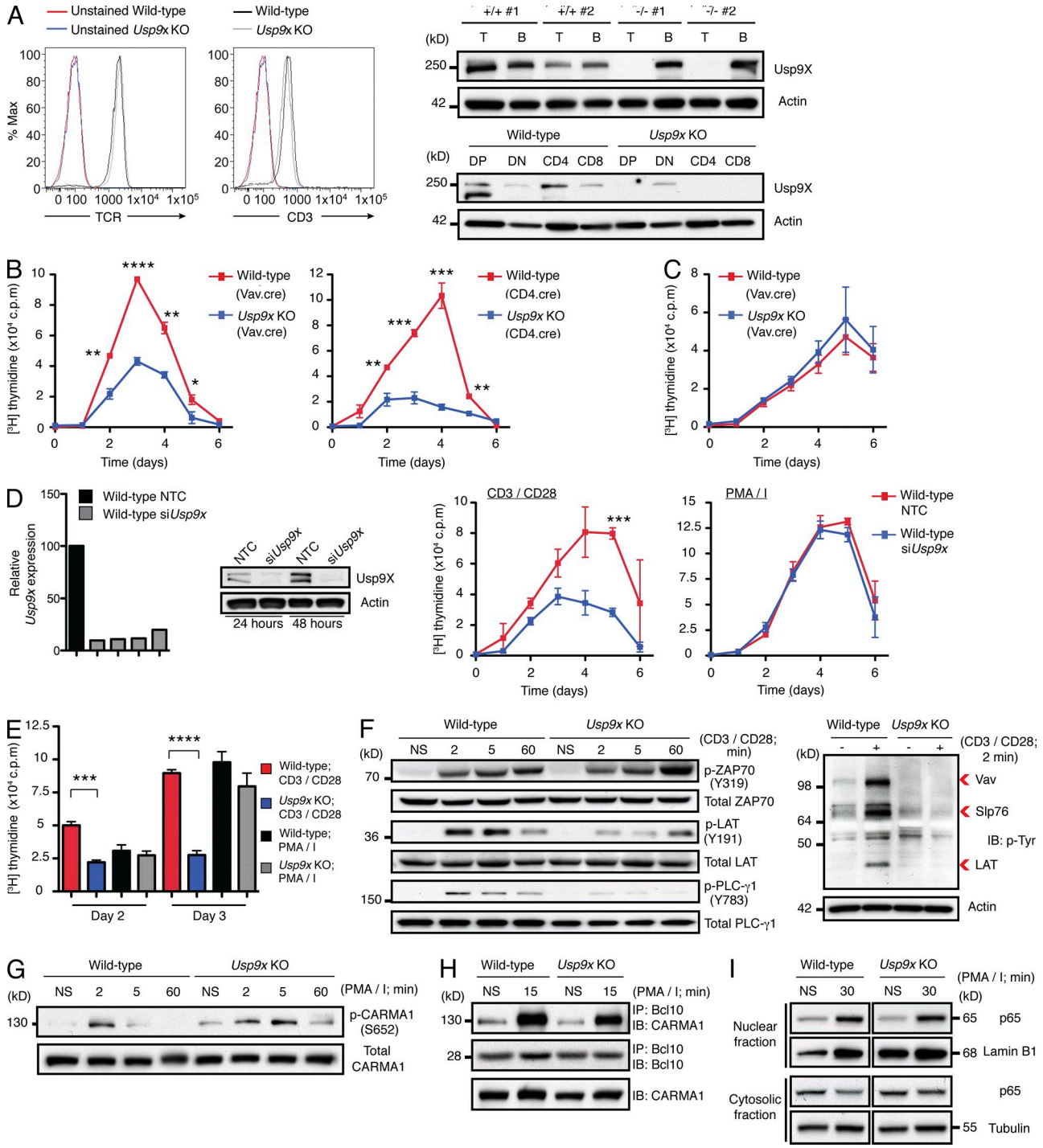

Figure 2. Usp9X regulates proximal TCR signaling events. (A) Representative histograms of TCR and CD3 levels on naive CD4+ T cells purified from CD4.cre mice. The specificity (T vs. B lymphocytes) and kinetics of deletion using CD4.cre was confirmed by Western blot. (B) Naive CD4+ T cell proliferation in response to CD3/CD28. Data represents mean ± SEM of 5–7 independent mice per genotype/time point. (C) Naive CD4+ T cell proliferation in response to PMA/ionomycin. Data represents mean ± SEM of 7–11 independent mice per genotype/time point. (D) Proliferation of wild-type T cells transfected with a nontargeting control (NTC) or *Usp9x* siRNAs (si*Usp9x*) that effectively reduced both *Usp9x* mRNA and protein levels. Data represent mean ± SEM of three independent transfections. (E) CD8+ (CD4.cre) T cell proliferation. Data represents mean ± SEM of 3 independent mice per genotype. (F and G) Naive CD4+ T cells (CD4.cre) were stimulated for the indicated times and proteins were fractionated and probed with the indicated antibodies. N.S., nonstimulated. The induction of tyrosyl-phosphorylated proteins was monitored with a phospho-tyrosine (p-Tyr)-specific antibody. (H) CBM complex formation in naive CD4+ T cells (CD4.cre) was assessed by co-immunoprecipitation of CARMA1 with Bcl10. (I) Nuclear translocation of the p65 subunit of NF-κB was monitored by subcellular fractionation of naive CD4+ T cells. DP, double-positive; DN, double-negative. *, P ≤ 0.05; **, P ≤ 0.01; ***, P ≤ 0.001; and ****, P ≤ 0.0001 of wild-type versus *Usp9x* KO using a two-tailed unpaired Student's *t* test. PMA/I, PMA/ionomycin. c.p.m., counts per minute.

Usp9x deficiency expands antigen-experienced, PD-1, and OX40-expressing T cell populations in vivo

Next, we assessed how the reduced signaling capacity of *Usp9x* KO T cells influenced T cell homeostasis in the whole animal. Unless specified, all subsequent analyses were conducted with the T cell–specific deleter strain CD4.cre. At 12 wk of age, *Usp9x* KO mice contained approximately threefold more $CD4^+$ $CD62L^-$ $CD25^-$ $CD44^{hi}$ antigen-experienced (effector–memory) T cells in the spleen and lymph nodes than their WT counterparts (Fig. 3 A), an expansion evident as early as 4 wk of age (Fig. 3 C). The number of naive $CD8^+$ T cells were also reduced in *Usp9x* KO mice (Fig. 3 B). Consequently, the ratio of both $CD4^+$ and $CD8^+$ memory to naive T cells was consistently elevated in *Usp9x* KO mice (Fig. 3, A and B).

To gain further insight into the defects caused by Usp9X deficiency, WT and *Usp9x* KO total T cells freshly isolated from 8–12-wk-old CD4.cre mice were analyzed by RNA sequencing. Interestingly, *Usp9x* KO cells expressed 3.6-fold more *Pdcd1* mRNA encoding the inhibitory receptor PD-1 than did WT cells. Consistent with this result, *Usp9x* KO mice contained ∼10-fold more PD-$1^{+/high}$ memory cells in the spleen than WT control mice, and numbers in the lymph nodes were also elevated (Fig. 3 D). Expression of *Tnfrsf4* encoding the stimulatory receptor OX40 was also increased in *Usp9x* KO T cells. By flow cytometry, *Usp9x* KO spleens and lymph nodes contained more memory $CD4^+$ cells that were $OX40^+$ (Fig. 3 E). OX40 provides co-stimulatory signals for a sustained T cell response (Croft et al., 2009), is up-regulated in several human autoimmune diseases, and therefore is indicative of generalized immune hyperactivity.

Usp9x deficiency in T cells causes spontaneous lupuslike autoimmunity and lymphoproliferative disease

Given the skewing of T cell subsets in the *Usp9x* KO mice, we monitored a cohort of aging CD4.cre mice for signs of autoimmunity. Unlike control mice, *Usp9x* KO mice exhibited progressive splenomegaly (Fig. 4 A) due to increased numbers of $CD4^+$ T cells, monocytes, and B cells (Fig. 4 B) and significant thymic hypertrophy due to infiltration of activated T cells and B cells from the perithymic lymph nodes (Fig. 4 A and not depicted). Of note, spleens from mice where Usp9X had been deleted specifically in B cells (using CD19.cre) were not significantly larger than control spleens (Fig. 4 C), revealing that a T cell–intrinsic defect was the primary driver of the pathology observed. Elevation of dsDNA autoantibodies (Fig. 4 D) and the presence of hypergammaglobulinemia, specifically of the IgG class (Fig. 4 E), were consistent with systemic lupus erythematosus (SLE)–like disease. Although SLE is classically viewed as a B cell–driven disease, emergent evidence confirms that T cells are crucial for enhancing autoantibody production by providing the signals that B cells require to differentiate, proliferate, and mature (Shlomchik et al., 2001).

Multiple visceral organs of *Usp9x* KO mice contained more perivascular and periductular lymphoplasmacytic cuffs in comparison to control mice (Fig. 4 F). Many aggregates contained a high proportion of plasma cells, including Mott cells that contain cytoplasmic immunoglobulin inclusions. Although glomerulonephritis is relatively common in older C57BL/6 mice, 7 out of 7 40–48-wk-old female *Usp9x* KO mice had severe disease compared with only 1 out of 5 WT mice. By 40 wk of age, *Usp9x* KO mice exhibited hallmarks

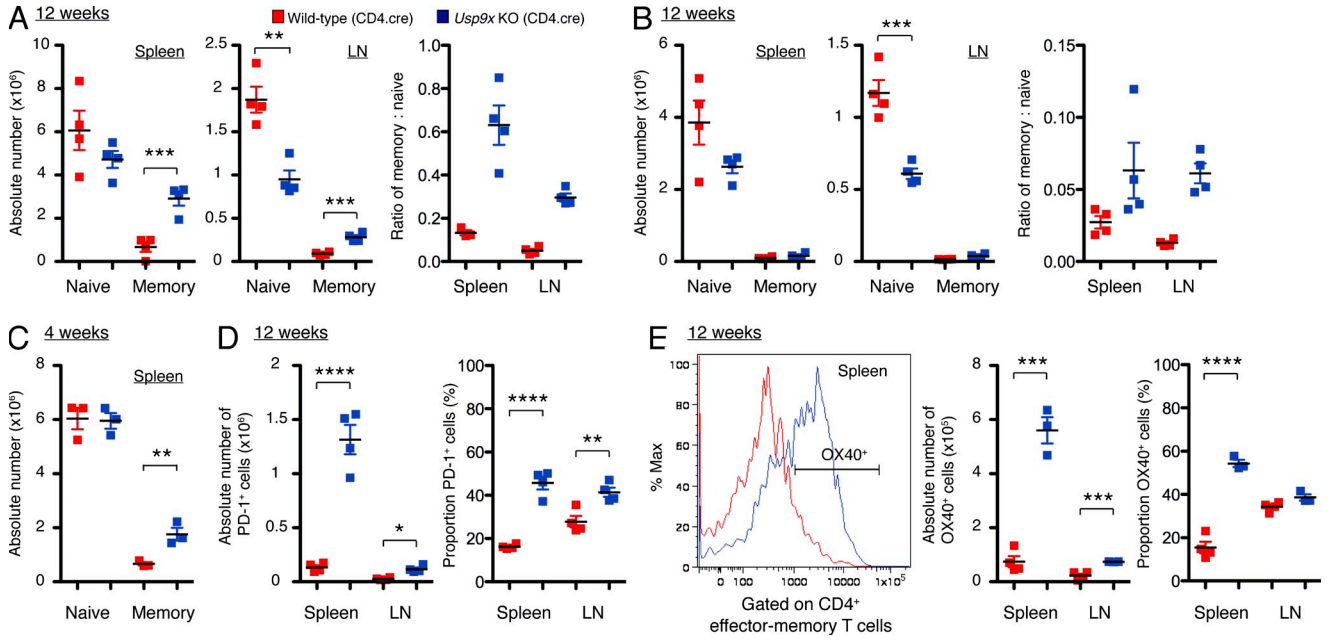

Figure 3. ***Usp9x*** **deficiency expands antigen-experienced, PD-1, and OX40-expressing T cell populations in vivo.** The number of naive or effector–memory $CD4^+$ (A and C) or $CD8^+$ (B) T cells in the spleens and LNs of CD4.cre mice. (D) Expansion of PD-1–expressing $CD4^+$ effector–memory populations in *Usp9x* KO spleens and LNs. (E) Representative histogram depicting OX40 expression on $CD4^+$ effector–memory T cells and the proportion and total number of $OX40^+$ memory T cells. *, $P \le 0.05$; **, $P \le 0.01$; ***, $P \le 0.001$; and ****, $P \le 0.0001$ of wild-type versus *Usp9x* KO using a two-tailed unpaired Student's *t* test.

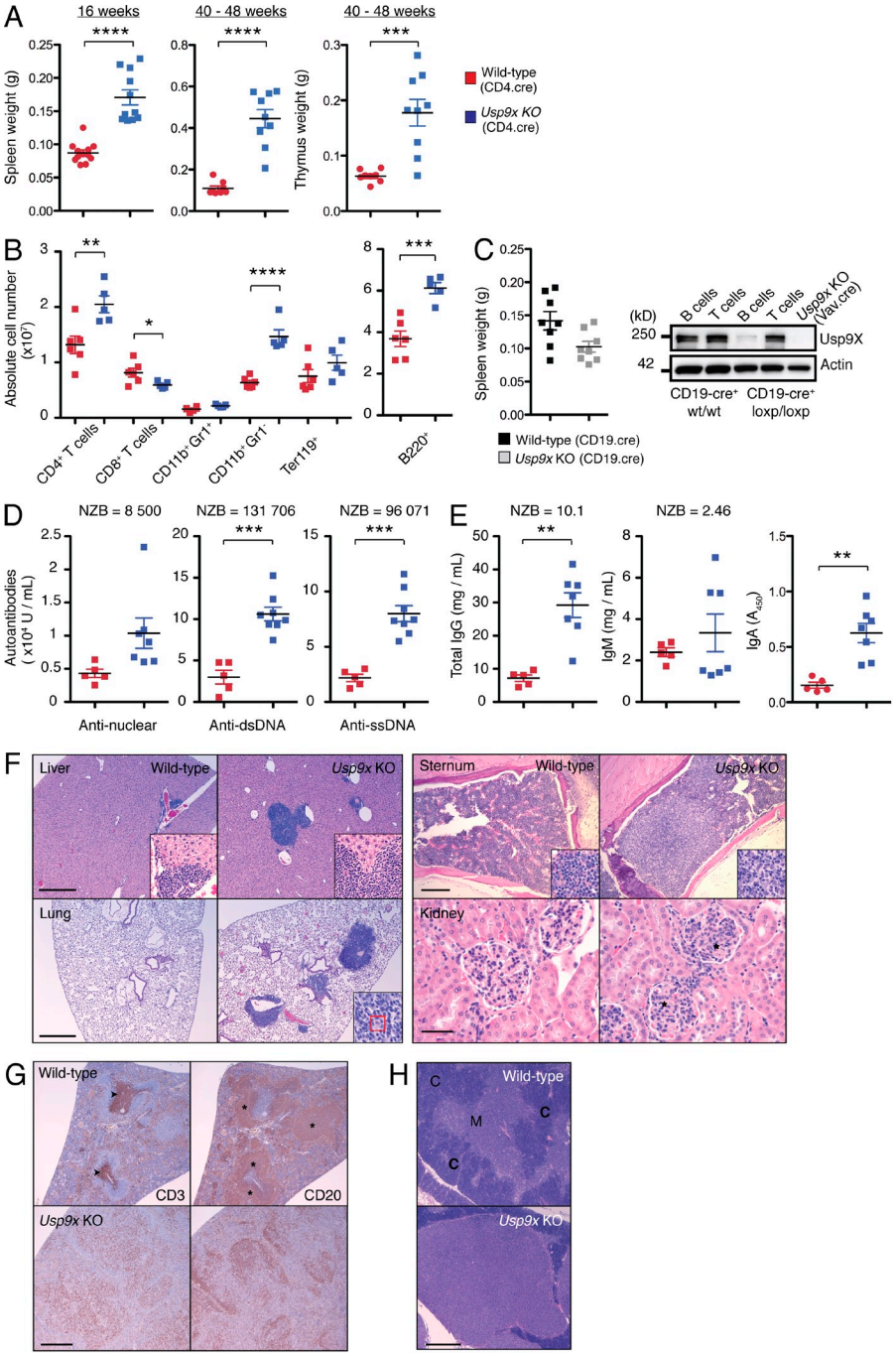

Figure 4. *Usp9x* KO mice develop spontaneous lupuslike autoimmunity and lymphoproliferative disease. (A) Mass of wild-type or *Usp9x* KO (CD4.cre) spleens and thymi. (B) Cell subset analysis of 16-wk-old mice. (C) Spleen mass of CD19.cre mice. The specificity of CD19.cre deletion was confirmed by Western blot. (D) Quantitation of serum ANA, double-strand DNA (dsDNA) and single-strand DNA (ssDNA) autoantibody levels by ELISA. (E) IgG, IgM, and IgA levels were quantitated in the sera using ELISA. Where indicated, serum from a New Zealand Black/White (NZB/W) F1 hybrid mouse with proteinuria served as a positive control. (F) Histopathological analysis of organs from 32-wk-old wild-type or *Usp9x* KO mice. The red box delineates a Mott cell and the asterisks denote areas of expanded mesangium consistent with membranoproliferative glomerulonephritis. Bars: (lung and liver) 500 µm; (sternum) 200 µm; (kidney) 50 µm. (G) CD3 and CD20 expression in the spleens of 48-wk-old mice revealed loss of normal tissue architecture, including periarteriolar lymphoid sheaths (arrowheads) and lymphoid follicles (asterisks). bar, 500 µm. (H) Absence of the cortical/medullary boundary in the thymi of 48-wk-old *Usp9x* KO mice. C, cortex; M, medulla. Bar, 500 µm. All experiments were conducted a minimum of two independent times with littermate controls on a C576BL/6 background. Each square represents an independent mouse. *, $P \leq 0.05$; **, $P \leq 0.01$; ***, $P \leq 0.001$; and ****, $P \leq 0.0001$ of wild-type versus *Usp9x* KO using a two-tailed unpaired Student's *t* test.

of lymphoproliferative disease similar to what is observed for autoimmune lymphoproliferative syndrome (ALPS) patients (Rieux-Laucat et al., 2003; Worth et al., 2006). CD3 and CD20 staining revealed that in addition to marked expansion of the splenic white pulp, *Usp9x* KO spleens had lost the normal architecture, including the well-defined periarteriolar lymphoid sheaths and lymphoid follicles (Fig. 4 G). Marked lymphoid expansion was also evident in the thymus, resulting in obliteration of the cortical/medullary boundary (Fig. 4 H). The fact that these lesions consisted of a heterogeneous population of T and B cells suggested that this was a hyperplastic rather than neoplastic process.

Defective intrathymic T cell development in the absence of Usp9X

Defects in T cell development in the thymus may drive autoimmunity in *Usp9x* KO mice. Normally, a strong TCR–MHC interaction causes deletion of autoreactive T cells, whereas a weaker interaction promotes the maturation of double-positive (DP) thymocytes into either CD4 or CD8 single-positive (SP) thymocytes

(Jameson et al., 1995; Kisielow and von Boehmer, 1995; Alam et al., 1996). A preTCR complex coupled to an intracellular signaling pathway resembling that present in mature T cells is also required for immature double-negative (DN) thymocytes to transition to the DP stage (Groves et al., 1996; Cheng et al., 1997; Pivniouk et al., 1998; Zhang et al., 1999). Given that TCR-induced activation and phosphorylation of ZAP70 substrates was perturbed in *Usp9x* KO DP thymocytes (Fig. 5, A and B), we hypothesized that both these processes would be affected.

Deletion of *Usp9x* at all stages of thymocyte development (with *vavCre*) resulted in fewer thymocytes at the DN4 stage and an overall reduction in thymic cellularity (Fig. 5 C). *Usp9x* KO CD69$^+$ DP thymocytes also expressed less Bim than their WT counterparts (Fig. 5 D). Bim is the proapoptotic protein required for the death of autoreactive T cells (Liston et al., 2004; Baldwin and Hogquist, 2007), so these data are consistent with impaired negative selection. Deletion of *Usp9x* during the DN-to-DP transition with CD4.cre (Fig. 2 A) yielded a greater proportion of CD4 and CD8 SP thymocytes (Fig. 5 E). Consistent with a selection shift model (Sakaguchi et al., 2003; Fig. 5 F), the increase in the proportion of SP cells in these animals is likely to reflect the fact that fewer thymocytes had reached the threshold for negative selection and, as a consequence, fewer T cells bearing autoreactive TCRs were eliminated.

In sum, we show that Usp9X is required for normal T cell development and proliferation. Inherited mutations causing primary human immunodeficiency are rare, so analyses of genetic alterations such as T cell–specific deletion of *Usp9x* that subtly reduce TCR signal strength may inform our understanding of a greater proportion of human immunopathology.

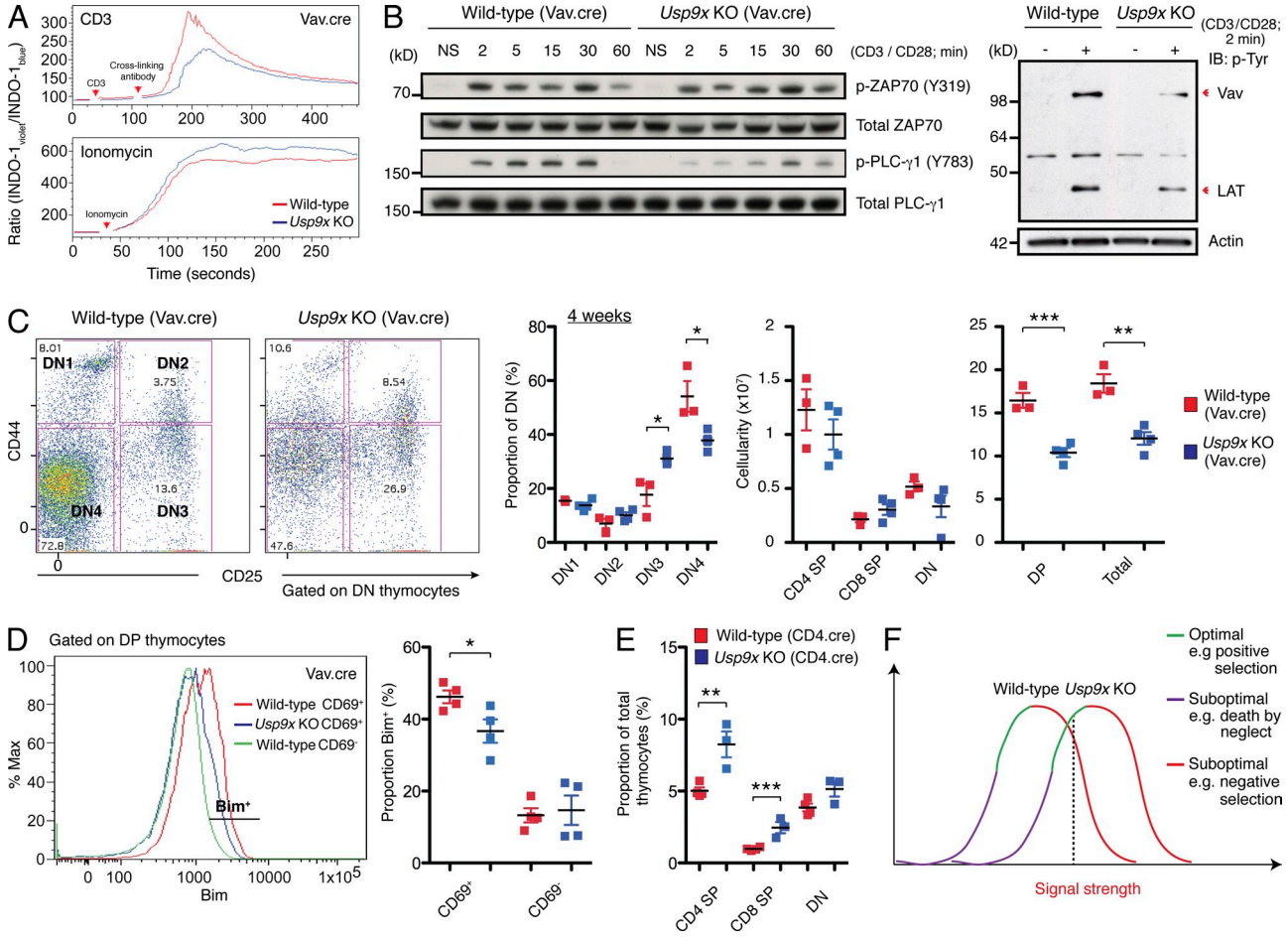

Figure 5. Defective T cell development in *Usp9x* KO mice. (A) Thymocyte activation was assessed by the degree of calcium flux elicited by cross-linked anti-CD3 antibody or the calcium ionophore ionomycin. Data are representative of three independent mice per genotype. (B) Western blot analysis confirmed that *Usp9x* KO thymocytes exhibit similar signaling defects to peripheral T cells. (C) Immature thymic subsets in the Vav.cre strain were enumerated using CD25 and CD44 co-staining to track the transition from DN1 to DN4 before differentiation in to DP thymocytes. (D) Intracellular FACS analysis of the proapoptotic molecule Bim in 4-wk-old Vav.cre mice. (E) Analysis of thymic subsets in 12-wk-old CD4.cre mice. (F) Graphical representation of the selection shift hypothesis. The dashed line denotes a signal strength that in wild-type T cells would result in deletion but in *Usp9x* KO T cells, results in positive selection. All experiments were conducted a minimum of two independent times with littermate controls on a C576BL/6 background. Each square represents an independent mouse. *, P ≤ 0.05; **, P ≤ 0.01; ***, P ≤ 0.001; and ****, P ≤ 0.0001 of wild-type versus *Usp9x* KO using a two-tailed unpaired Student's *t* test.

MATERIALS AND METHODS

Mice. The loxP-targeted allele of Usp9X was generated by Lexicon using C57BL/6 embryonic stem cells and standard molecular biology techniques. The loxP sites flank exon 31 of *Usp9X*. *Usp9X*$^{fl/fl}$ mice were crossed to C57BL/6-*Gt(ROSA)26Sor*$^{tm16(Cre)Arte}$ (Taconic), Tg(Vav1-cre)1Cgp (MGI ID: 5527187), or B6.Cg-Tg(CD4.cre)1Cwi N9 (Taconic) deleter strains and backcrossed to a C57BL/6 background for >10 generations. The complete open reading frame of the tdTomato fluorescent protein and a T2A sequence was inserted between the 5′ untranslated region (UTR) and the translation initiation codon present in exon 2 of *Usp9X*. B6. 129S6-*Rag2*^{tm1Fwa}N12 mice were purchased from Taconic. *Usp9X*^{fl} genotyping primers 5′-GGCAGGTATTCCCACTCAGTAAGTG-3′ and 5′-TGCTGTCTTAAATGCATTTATTAATGGAG-3′ amplified 175-bp (WT) and 260-bp (LoxP) genomic DNA fragments. *Usp9X*.tdTomato knock-in (KI) genotyping primers 5′-AGGAGGGCAGAGGAAGTC-3′, 5′-CAATGTTGATTTCAGCACCTAAGT-3′, and 5′-TGCCCTGTGTCGAGTATGA-3′ amplified 283-bp (WT) and 324-bp (KI) genomic DNA fragments. All experiments were conducted with the approval of the Genentech Institutional Animal Care and Use Committee.

Cell surface and intracellular staining and FACS. Fluorescent antibodies to cell surface antigens were diluted 1/50 in 1 μg/ml CD16/CD32 (BD; 553142) to block F_c receptors, 10% FCS/PBS and incubated with cells for 30 min on ice. Before analysis, cells were resuspended in 2 μg/ml propidium iodide (BD; 556463) to exclude dead cells. For quantitation of total cell number, a defined number of unlabeled Calibrite beads (BD; 349502) were added per sample and numbers calculated according to the following equation: (total no. of beads/no. of gated beads) × no. of gated cells. For absolute number per organ, the total cell number was multiplied by the dilution factor. Data were obtained using a LSR II Flow Cytometer (BD) and all post-acquisition analyses were performed in FlowJo (v8.4.5). The following antibodies were used for multiparameter FACs analysis and cell sorting and were all purchased from BD with the exception of F4/80: B220 (RA3 – 6B2), CD3 (145-2C11), CD4 (H129-19), CD8 (53–6.7), CD11b (M1/70), CD11c (HL3), CD19 (ID3), CD24 (M1/69), CD25 (PC61), CD41 (MWReg30), CD44 (IM7), CD62L (MEL14), CD46RB (16A), CD69 (H1.2F3), c-kit (2B8), F4/80 (eBioscience; clone BM8), Gr-1 (R.86-8C5), OX40 (OX-86), PD-1 (J43), Sca-1 (D7), and Ter-119 (TER-119). For detection of biotinylated antibodies, samples were incubated with a 1/250 dilution of streptavidin-PE (BD; 554061) for 15 min on ice. The following cell surface immunophenotypes were used to define the subsets in Fig. 1. Lineage-negative cells were obtained by magnetic bead isolation from the bone marrow using Lineage Depletion kit (Miltenyi Biotec) before cell surface staining. HSC: Lin$^-$ Sca-1$^+$ c-kit^{Hi}; CMP: Lin$^-$ Sca-1$^-$ c-kit^{Hi}; CLP: Lin$^-$ Sca-1^{lo} c-kit^{lo}; Mac: F4/80$^+$; Gran: CD11b$^+$ Gr-1$^+$; Plat: CD41$^+$ CD62L$^+$; Den: CD11c$^+$; T: CD3$^+$; and B: CD19$^+$ B220$^+$. The following immunophenotypes were used to define the DN1-to-DN4 thymocyte populations: DN1, CD44^{Hi} CD25$^-$; DN2: CD44^{Hi} CD25$^+$; DN3: CD44$^-$ CD25$^+$; and DN4: CD44$^-$ CD25$^-$. Following CD4, CD8 and CD69 cell surface staining, cells were fixed in 1% paraformaldehyde for 15 min at room temperature and intracellular Bim expression detected by incubation with 5 μg/ml of Bim (Enzo Life Sciences; clone 3C5) in 50 μg/ml CD16/CD32/0.3% saponin (staining buffer). All subsequent washes were performed with 10% FCS/PBS/0.03% saponin. Samples were resuspended in biotinylated mouse anti–rat IgG_{2a} (Southern Biotech) at 10 μg/ml in staining buffer, vortexed rigorously, and incubated on ice for 30 min followed by a 30-min incubation with a 1/50 dilution of streptavidin-FITC (BD).

Lymphocyte purification and thymidine proliferation assay. Naive CD4$^+$ T cells were purified from homogenized spleens using magnetic bead selection to deplete non-T and CD8$^+$ T cell populations and CD62L for positive selection of naive cells (Miltenyi Biotec). CD8$^+$ and total T cells were purified by magnetic depletion (Miltenyi Biotec). All procedures were performed in accordance with the manufacturer's protocols. Purity was typically >90% for both wild-type and *Usp9x* KO samples. For proliferation assays using CD4.cre mice, T cells were sorted using a FACSAria (BD) to obtain CD4$^+$ CD62L$^+$ CD44^{lo} CD25$^-$ naive T cells with purity typically >99%. Purified cells were seeded at 10^5C/100 μl/well in a U-bottom 96-well microtiter plate (Costar; 3799). For polyclonal T cell activation using CD3/CD28 antibodies, plates were coated with 5 μg/ml of anti-CD3 (BD; clone 145-2C11) and 10 μg/ml anti-CD28 (BD; clone 37.51) overnight at 4°C and washed three times with PBS before the addition of purified cells in T cell culture medium (10% heat-inactivated FCS, penicillin, streptomycin, nonessential amino acids, L-Glutamine, sodium pyruvate, and 50 μM 2-β-mercaptoethanol) and incubation at 37°C/5% CO_2. Cells were treated with 10 ng/ml PMA and 0.5 μM ionomycin and plated as described above. At the indicated times, 0.5 μCi of tritiated thymidine was added to each well and allowed to incorporate for 24 h before harvesting on to a Unifilter-96, GF/C microplate (Perkin Elmer). Counts were obtained by the addition of scintillation fluid and analysis using a TopCount microplate scintillation reader (Perkin Elmer).

Biochemical analyses. For signaling studies, purified T cells were rested for 1 h in complete medium at 37°C/5% CO_2 before stimulation with CD3/CD28-coated microbeads (Dynabeads Mouse T cell activator). Cells were lysed in RIPA lysis buffer (50 mM Tris, pH 7.4, 150 mM NaCl, 2 mM EDTA, 1% NP-40, and 0.1% SDS) supplemented with protease (Roche) and phosphatase inhibitors (Roche). After clarification of the lysates by centrifugation, protein concentrations were determined using the BCA protein quantitation assay (Thermo Fisher Scientific). Between 15 and 50 μg of total protein and a prestained molecular weight marker (Novex; LC5625) were separated using SDS-PAGE electrophoresis. Western blots were probed with the following antibodies: Usp9X (Genentech; clone 4B3.1.1), phospho-ZAP70 (Cell Signaling Technology), total ZAP70 (Cell Signaling Technology), phospho-LAT (Cell Signaling Technology), total LAT (Cell Signaling Technology), phospho-PLC-γ1 (Cell Signaling Technology), total PLC-γ1 (Cell Signaling Technology), phospho-CARMA1 (Cell Signaling Technology), total CARMA1 (Cell Signaling Technology), total Bcl10 (Cell Signaling Technology), total p65 (Cell Signaling Technology), total Lamin B1 (Cell Signaling Technology), total tubulin (Cell Signaling Technology), phosphotyrosine (Cell Signaling Technology; clone P-Tyr-100), and β-actin (Novus Biologicals; clone AC-15). Where applicable, antibodies were detected using a 1:2,500 dilution of HRP-conjugated anti–rabbit IgG secondary (Cell Signaling Technology) or HRP-conjugated anti–rat IgG secondary (Santa Cruz Biotechnology, Inc.). For co-immunoprecipitation studies, cells were lysed in Triton lysis buffer (50 mM Tris-Cl, pH 7.4, 150 mM NaCl, 1 mM EDTA, and 1% Triton) supplemented with inhibitors and clarified as described above. Between 0.5 and 1 mg of total protein was diluted in lysis buffer to a final concentration of 1 mg/ml, 3 μg of Bcl10 (SC-5273; Santa Cruz Biotechnology, Inc.) was added, and samples incubated overnight rotating at 4°C. The following day, 40 μl of a 50% slurry of anti–mouse IgG-agarose beads (Sigma-Aldrich) was incubated for 4 h rotating at 4°C. Samples were washed and bound proteins were eluted by boiling in SDS sample buffer. Subcellular fractionation was performed using a commercially available kit according to the manufacturer's instructions (Thermo Fisher Scientific; NE-PER kit).

Calcium flux. Naive CD4$^+$ T cells were resuspended at 5 × 10^6 cells per ml in room temperature loading buffer (0.5% BSA/HBSS with magnesium and calcium). INDO-1 (Life Technologies; I-1223) was added to a final concentration of 2 μg/ml and samples incubated in a 37°C waterbath for 30 min. Samples were centrifuged for 6 min at 180 *g* and resuspended at 3 × 10^6 C/ml in loading buffer supplemented with 2 μg/ml propidium iodide. A baseline reading was taken for 30 s before the addition of 10 μg/ml of anti-CD3 antibody. After a further 60 s of equilibration, 100 μg/ml of goat anti–hamster cross-linking secondary (Vector Laboratories) was added and the degree of calcium flux quantitated by the change in the ration of INDO-1^{violet}/INDO-1^{blue}. Naive T cells were loaded with INDO-1 and a baseline reading obtained for 30 s before the addition of 2 μg/ml of ionomycin. A Fortessa FACS machine (BD) with a UV excitation filter was used to acquire this data.

Autoantibody and immunoglobulin ELISAs. Blood was collected by cardiac puncture and serum obtained using Microtainer Serum Separator Tubes

(BD). ELISA kits for autoantibody detection were purchased from Alpha Diagnostics. Serum was diluted 1/100 in low NSB sample diluent for all autoantibody ELISAs. Units per ml were determined with reference to a standard curve. ELISA kits from Abcam were used to assess immunoglobulin levels in serum diluted between 1:20,000 and 1:50,000. All kits were used according to the manufacturer's instructions. Total levels were determined with reference to a standard curve, whereas absorbance at 450 nM was used to compare the levels of IgA. Absorbance readings at 450 nM were obtained using a SpectraMax 190 microplate reader (Molecular Devices) and absolute concentrations calculated using SoftMaxPro software (Molecular Devices).

Immunohistochemistry and immunofluorescence. CD3 and CD20 immunohistochemistry was performed on paraffin-embedded sections of pancreas, thymus, lung, liver, kidney, heart, mesenteric lymph node, spleen, and sternum. The slides were processed by an autostainer (Dako) with manufacturer's target retrieval before a 60-min incubation with a 1/200 dilution of CD3 (Thermo Fisher Scientific; clone SP7), 2 µg/ml CD20 (Thermo Fisher Scientific), or 2 µg/ml naive rabbit IgG (polyclonal) as a negative control. The ABC-peroxidase Elite kit (Vector Laboratories) with 3, 3′–Diaminobenzidine (DAB) as the chromogen was used as the detection system. Hematoxylin and eosin–stained sections were obtained by standard histochemical techniques.

RNaseq. RNA was extracted from total peripheral T cells using RNeasy Mini kits (QIAGEN) with on-column DNase treatment. 5 µg of pooled RNA (n > 15 mice per genotype) was submitted for analysis using the Illumina HiSeq 2000 platform. RNaseq reads were first aligned to ribosomal RNA sequences to remove ribosomal reads. The remaining reads were aligned to the human reference genome (NCBI Build 37) using GSNAP version 2011-12-28, allowing maximum of 3 mismatches per 100 base sequence (parameters: -M 2 -n 10-B 2-i 1-N 1-w 200000-E 1–pairmax-rna = 200,000). Transcript annotation was based on the RefSeq database downloaded on 11/30/2011. To quantify gene expression levels, the number of reads mapped to the exons of each RefSeq gene was calculated. Differential expression analysis on the count data were performed using the R package DESeq, which is based on a negative binomial distribution and uses shrinkage estimation for the variance of the distribution.

siRNA-mediated knock-down. Total T cells isolated from C57BL/6 wild-type mice by magnetic bead negative selection (Miltenyi Biotec) were transfected with 600 pmol siRNA using the Amaxa Mouse T cell Nucleofector kit and according to the manufacturer's instructions (Lonza). Transfected cells were rested for 2 h before stimulation and assessment of proliferation as described previously. Chemically modified siRNAs were generated as previously described (Mantei et al., 2008) and their sequences are as follows: 5′-3′ nontargeting control, sense 5′-GmGmAGCGCACCAUCUUCTdCdAdAmUmUm-3′, antisense 5′-AdUUGAGAAGAUGGUGCGCUCmCm-3′; Usp9X (1) 5′-AmAmCCAAGUAACUCAUGATdCdAdAmGmCm-3′, antisense 5′-TdUGAUCAUGAGUUACUUGGUmUm-3′; Usp9X (2), sense 5′-CmCmCAAAUGAAGAAGUGACdAdAdAmAmAm-3′, antisense 5′-TdUUGUCACUUCUUCAUUUGGmGm-3′, Usp9X (3), 5′-UmUmUGAAUUUCCUCGAGAGdTdTdAmGmAm-3′, antisense 5′-TdAACUCUCGAGGAAAUUCAAmAm-3′; Usp9X (4), 5′-CmUmUGGCAAAGUUAGAUGAdTdAdUmGmAm-3′, antisense 5′-AdUAUCAUCUAACUUUGCCAAmGm-3′. Cm, Um, Am, Tm, or Gm denote a methoxy nucleotide and Gd, Ad, Td, or Cd denote a deoxynucleotide.

Image acquisition and processing. Hematoxylin and eosin stained histological, and CD3 and CD20 immunohistochemically labeled tissue sections were imaged with a Leica DM600 B brightfield microscope at ambient room temperature. Photomicrographs were acquired using a Leica DFC 500 camera in conjunction with Leica Application Suite software. Histological sections of the liver, lung, thymus, and immunohistochemical sections of the spleen were acquired with a 5×/0.15 NA objective, and insets of the liver and lung were acquired with a 20×/0.7 NA objective. Photomicrographs of sternums were acquired with a 10×/0.4 NA objective, and the insets of the sternum and photomicrographs of glomeruli were acquired with a 40×/0.85 NA objective.

Statistical analysis. Statistical comparisons were made in Prism (v.5.0d) using a two-tailed unpaired Student's t test. P-values <0.05 were deemed significant.

We thank Sascha Rutz for advice regarding the use of chemically stabilized siRNAs, Hanne Van Korp for the calcium flux protocol, Wyne Lee for provision of NZB/W F1 hybrid sera and kidneys, and Felix Chu for CD3 and CD20 immunohistochemistry. We also thank Nobuhiko Kayagaki and Kim Newton for critical discussions, Kim Newton for help with manuscript preparation and Laszlo Komuves for imaging support. We thank the Next-generation sequencing, necropsy, histology and FACS staff at Genentech for their technical support.

The authors declare no additional competing financial interests.

Submitted: 5 May 2014
Accepted: 11 August 2014

REFERENCES

Al-Hakim, A.K., A. Zagorska, L. Chapman, M. Deak, M. Peggie, and D.R. Alessi. 2008. Control of AMPK-related kinases by USP9X and atypical Lys(29)/Lys(33)-linked polyubiquitin chains. *Biochem. J.* 411:249–260. http://dx.doi.org/10.1042/BJ20080067

Alam, S.M., P.J. Travers, J.L. Wung, W. Nasholds, S. Redpath, S.C. Jameson, and N.R. Gascoigne. 1996. T-cell-receptor affinity and thymocyte positive selection. *Nature*. 381:616–620. http://dx.doi.org/10.1038/381616a0

Baldwin, T.A., and K.A. Hogquist. 2007. Transcriptional analysis of clonal deletion in vivo. *J. Immunol.* 179:837–844. http://dx.doi.org/10.4049/jimmunol.179.2.837

Cheng, A.M., I. Negishi, S.J. Anderson, A.C. Chan, J. Bolen, D.Y. Loh, and T. Pawson. 1997. The Syk and ZAP-70 SH2-containing tyrosine kinases are implicated in pre-T cell receptor signaling. *Proc. Natl. Acad. Sci. USA*. 94:9797–9801. http://dx.doi.org/10.1073/pnas.94.18.9797

Croft, M., T. So, W. Duan, and P. Soroosh. 2009. The significance of OX40 and OX40L to T-cell biology and immune disease. *Immunol. Rev.* 229:173–191. http://dx.doi.org/10.1111/j.1600-065X.2009.00766.x

Dupont, S., A. Mamidi, M. Cordenonsi, M. Montagner, L. Zacchigna, M. Adorno, G. Martello, M.J. Stinchfield, S. Soligo, L. Morsut, et al. 2009. FAM/USP9x, a deubiquitinating enzyme essential for TGFbeta signaling, controls Smad4 monoubiquitination. *Cell*. 136:123–135. http://dx.doi.org/10.1016/j.cell.2008.10.051

Groves, T., P. Smiley, M.P. Cooke, K. Forbush, R.M. Perlmutter, and C.J. Guidos. 1996. Fyn can partially substitute for Lck in T lymphocyte development. *Immunity*. 5:417–428. http://dx.doi.org/10.1016/S1074-7613(00)80498-7

Jameson, S.C., K.A. Hogquist, and M.J. Bevan. 1995. Positive selection of thymocytes. *Annu. Rev. Immunol.* 13:93–126. http://dx.doi.org/10.1146/annurev.iy.13.040195.000521

Kisielow, P., and H. von Boehmer. 1995. Development and selection of T cells: facts and puzzles. *Adv. Immunol.* 58:87–209. http://dx.doi.org/10.1016/S0065-2776(08)60620-3

Komander, D., and M. Rape. 2012. The ubiquitin code. *Annu. Rev. Biochem.* 81:203–229. http://dx.doi.org/10.1146/annurev-biochem-060310-170328

Liston, A., S. Lesage, D.H. Gray, L.A. O'Reilly, A. Strasser, A.M. Fahrer, R.L. Boyd, J. Wilson, A.G. Baxter, E.M. Gallo, et al. 2004. Generalized resistance to thymic deletion in the NOD mouse; a polygenic trait characterized by defective induction of Bim. *Immunity*. 21:817–830.

Lupher, M.L. Jr., K.A. Reedquist, S. Miyake, W.Y. Langdon, and H. Band. 1996. A novel phosphotyrosine-binding domain in the N-terminal transforming region of Cbl interacts directly and selectively with ZAP-70 in T cells. *J. Biol. Chem.* 271:24063–24068. http://dx.doi.org/10.1074/jbc.271.39.24063

Mantei, A., S. Rutz, M. Janke, D. Kirchhoff, U. Jung, V. Patzel, U. Vogel, T. Rudel, I. Andreou, M. Weber, and A. Scheffold. 2008. siRNA stabilization prolongs gene knockdown in primary T lymphocytes. *Eur. J. Immunol.* 38:2616–2625. http://dx.doi.org/10.1002/eji.200738075

Nagai, H., T. Noguchi, K. Homma, K. Katagiri, K. Takeda, A. Matsuzawa, and H. Ichijo. 2009. Ubiquitin-like sequence in ASK1 plays critical roles in the recognition and stabilization by USP9X and oxidative stress-induced cell death. *Mol. Cell*. 36:805–818. http://dx.doi.org/10.1016/j.molcel.2009.10.016

Park, Y., H.S. Jin, and Y.C. Liu. 2013. Regulation of T cell function by the ubiquitin-specific protease USP9X via modulating the Carma1-Bcl10-Malt1 complex. *Proc. Natl. Acad. Sci. USA*. 110:9433–9438. http://dx.doi.org/10.1073/pnas.1221925110

Pivniouk, V., E. Tsitsikov, P. Swinton, G. Rathbun, F.W. Alt, and R.S. Geha. 1998. Impaired viability and profound block in thymocyte development in mice lacking the adaptor protein SLP-76. *Cell*. 94:229–238. http://dx.doi.org/10.1016/S0092-8674(00)81422-1

Rao, N., M.L. Lupher Jr., S. Ota, K.A. Reedquist, B.J. Druker, and H. Band. 2000. The linker phosphorylation site Tyr292 mediates the negative regulatory effect of Cbl on ZAP-70 in T cells. *J. Immunol.* 164:4616–4626. http://dx.doi.org/10.4049/jimmunol.164.9.4616

Rieux-Laucat, F., F. Le Deist, and A. Fischer. 2003. Autoimmune lymphoproliferative syndromes: genetic defects of apoptosis pathways. *Cell Death Differ.* 10:124–133. http://dx.doi.org/10.1038/sj.cdd.4401190

Ryan, M.D., A.M. King, and G.P. Thomas. 1991. Cleavage of foot-and-mouth disease virus polyprotein is mediated by residues located within a 19 amino acid sequence. *J. Gen. Virol.* 72:2727–2732. http://dx.doi.org/10.1099/0022-1317-72-11-2727

Sakaguchi, N., T. Takahashi, H. Hata, T. Nomura, T. Tagami, S. Yamazaki, T. Sakihama, T. Matsutani, I. Negishi, S. Nakatsuru, and S. Sakaguchi. 2003. Altered thymic T-cell selection due to a mutation of the ZAP-70 gene causes autoimmune arthritis in mice. *Nature*. 426:454–460. http://dx.doi.org/10.1038/nature02119

Schwickart, M., X. Huang, J.R. Lill, J. Liu, R. Ferrando, D.M. French, H. Maecker, K. O'Rourke, F. Bazan, J. Eastham-Anderson, et al. 2010. Deubiquitinase USP9X stabilizes MCL1 and promotes tumour cell survival. *Nature*. 463:103–107. http://dx.doi.org/10.1038/nature08646

Shlomchik, M.J., J.E. Craft, and M.J. Mamula. 2001. From T to B and back again: positive feedback in systemic autoimmune disease. *Nat. Rev. Immunol.* 1:147–153. http://dx.doi.org/10.1038/35100573

Wood, S.A., W.S. Pascoe, K. Ru, T. Yamada, J. Hirchenhain, R. Kemler, and J.S. Mattick. 1997. Cloning and expression analysis of a novel mouse gene with sequence similarity to the Drosophila fat facets gene. *Mech. Dev.* 63:29–38. http://dx.doi.org/10.1016/S0925-4773(97)00672-2

Worth, A., A.J. Thrasher, and H.B. Gaspar. 2006. Autoimmune lymphoproliferative syndrome: molecular basis of disease and clinical phenotype. *Br. J. Haematol.* 133:124–140. http://dx.doi.org/10.1111/j.1365-2141.2006.05993.x

Zhang, W., C.L. Sommers, D.N. Burshtyn, C.C. Stebbins, J.B. DeJarnette, R.P. Trible, A. Grinberg, H.C. Tsay, H.M. Jacobs, C.M. Kessler, et al. 1999. Essential role of LAT in T cell development. *Immunity*. 10:323–332. http://dx.doi.org/10.1016/S1074-7613(00)80032-1